

CSRRS FOR EFFICIENT REDUCTION OF THE ELECTROMAGNETIC INTERFERENCES AND MUTUAL COUPLING IN MICROSTRIP CIRCUITS

X. Han, H. Hafdallah Ouslimani^{*}, T. Zhang, and A. C. Priou

Energy Mechanical Electromagnetic Lab., LEME, Université Paris Ouest Nanterre La Défense, 50 rue de Sèvres, Ville d'Avray 92410, France

Abstract—This paper proposes an efficient microstrip isolator filter which suppresses the surface and lateral waves (SW and LW) in planar antenna arrays. The structure consists in a double or triple row of periodic and flipped array of subwavelength Complementary Split Ring Resonators (CSRRs). The array of CSRRs is etched on a dielectric substrate backed by a metallic ground plane. These structures can both block the electromagnetic (EM) energy in one direction and guide it along the other transverse direction. In particular, the flipped array of CSRRs presents wider bandgap characteristic (stopband $\geq 20\%$) than periodic array of CSRRs ($\sim 16\%$) and conventional array of SRRs ($\geq 12\%$). Then, the metamaterial filter is inserted between two 6.1 GHz probe-fed patch antenna elements separated by a distance of $0.8\lambda_0$. Excellent agreements between the simulated and the experimental results are obtained. In fact, a significant reduction of the EM mutual coupling is achieved, more than 24 dB, over a wide frequency bandwidth. Moreover, the proposed CSRR structures are compact, low complex and, as printed antennas, are very easy to manufacture. They have numerous applications in MIMO systems and directive phased arrays.

1. INTRODUCTION

Electromagnetic interferences (EMI) in high speed integrated circuits and microstrip antenna arrays have caused strong mutual coupling effects and crosstalk noise which affect and degrade significantly their intrinsic performances. As it is well known, these EMI effects between

Received 24 May 2012, Accepted 23 July 2012, Scheduled 24 July 2012

^{*} Corresponding author: Habiba Hafdallah Ouslimani (habiba.ouslimani@u-paris10.fr).

closely-spaced antenna arrays are particularly due to surface waves (or surface currents) and lateral waves (or space waves). Various techniques to reduce the mutual coupling between antennas have been proposed [1–25]. Some of them [1–10] have put in light the efficiency of the Mushroom EBG structures in eliminating the surface waves (SW) inside a specific frequency band. In their last paper, the authors [11–13] show the ability of a vertical wall array of grounded edge-coupled Split Ring Resonators (GE-SRR metamaterial Slab) to reduce the EM coupling effects and improve the performance of microstrip phased arrays. Due to the metamaterial (MTM) influence, the scanning properties of the phased arrays [13] are remarkably improved: in particular the suppression of the scan blindness and grating lobes with an extension of the scanning range due to wide-angle impedance matching. In [15], the insertion of a MTM SRR media with a negative permeability (or MNG inclusions) between closely-spaced (only $\lambda_0/8$) high-profile monopole MIMO antenna elements, reduces the mutual coupling by almost 20 dB at the resonant frequency while maintaining good impedance matching of the antennas.

A new metamaterial particle-based on the use of complementary split ring resonators (CSRRs) has been suggested for the first time by Falcone et al. [16]. This MTM structure has a negative permittivity feature and can be implemented by etching the CSRRs on the microstrip antenna's ground plane [16–21].

In this paper, we developed new isolator structures based on subwavelength CSRR particles in order to reduce the EMI. The Babinet's principle states the complementarity of magnetic and electric fields of a single SRR and its complementary screen, a CSRR [12, 21, 22]. Therefore, the CSRR behaves as an electric dipole excited by an electric field polarized in the axial direction of the ring. At the resonance, the MTM array of CSRRs has a negative permittivity and inhibits signal propagation. Indeed, the propagation constant is purely imaginary so all the waves which pass across the structure are evanescent waves [17, 19, 20]. Besides, the arrays of CSRRs are more suitable for application in low profile planar antenna arrays to improve the bandwidth of the decoupling effects and enhance their performances. In addition, the structures are compact, low complex and do not need metallic vias. So, CSRR can be easily fabricated using microstrip technology (etched on the same platforms than printed antennas).

Hence, five prototypes of two E -coupled patch antennas array with and without the new isolator structures have been elaborated and fully characterized. The simulated and the measured results are presented: over a large frequency bandwidth around the resonance,

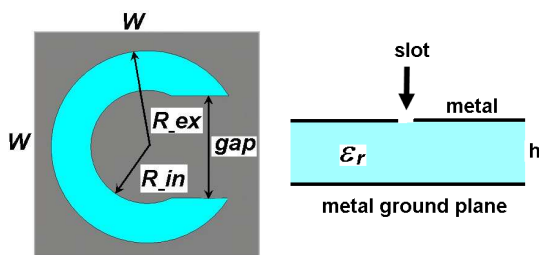


Figure 1. CSRR unit cell geometry and dimensions [$R_{in} = 2\text{ mm}$, $R_{ex} = 3.6\text{ mm}$, $gap = 3.6\text{ mm}$ and $W = 8\text{ mm}$]. Dielectric substrate $h = 1.9\text{ mm}$ thick, $\epsilon_r = 10.2$, loss tangent = $\tan(\delta) = 0.0023$.

EM mutual coupling effects are strongly reduced. Moreover, at the resonance frequency, the gain of the antenna is increased ($\sim 3\text{ dB}$ in broadside) due to the influence of the MTM isolator filter. The design model has been analyzed and optimized with the commercial software package HFSS 12.0 [26] and CST Microwave studio [27].

2. DESIGN AND CHARACTERIZATION OF THE UNIPLANAR CSRR STRUCTURES

2.1. Description of the Designed Structures

Figure 1 shows the Uniplanar CSRR unit cell (without vias). It is printed on a dielectric substrate [28] with 1.9 mm thick, relative dielectric permittivity ($\epsilon_r = 10.2$) and loss tangent ($\tan(\delta) = 0.0023$) backed by a metallic ground plane.

The CSRR structure has an electrical resonance excited by vertically polarized (with respect to the CSRR’s plane) electrical fields. The CSRR can be modeled as resonant structure of L_{CSRR} and C_{CSRR} [23, 18] with a resonant frequency given by (1) [18].

$$f_0 = \frac{1}{2\pi\sqrt{L_{CSRR} \times C_{CSRR}}} \tag{1}$$

The dimensions of the unit cell are optimized to operate around 6.1 GHz. The final values are indicated in Fig. 1 ($R_{in} = 2\text{ mm}$, $R_{ex} = 3.6\text{ mm}$, $gap = 3.6\text{ mm}$ and $W = 8\text{ mm}$). Fig. 2 shows the four proposed isolator structures composed by a double or triple row of seven CSRR unit particles. Two of them are organized in periodic array of CSRRs (shown in Figs. 2(a) and 2(c)). The others are flipped arrays of CSRRs (shown in Figs. 2(b) and 2(d)) developed to enlarge

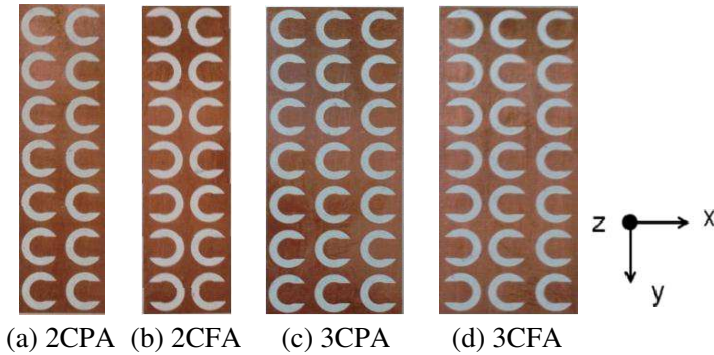


Figure 2. Fabricated MTM CSRR microstrip isolator filters, (a) 2 rows of periodic array of CSRRs (2CPA), (b) 2 rows of flipped array of CSRRs (2CFA), (c) 3 rows of periodic array of CSRRs (3CPA), and (d) 3 rows of flipped array of CSRRs (3CFA).

the filter's bandgap width. In the flipped array, the orientation of adjacent CSRR unit cells has been changed in the left row.

2.2. Numerical Study of the Designed CSRR Structures

The propagation properties of the MTM structures are numerically analyzed under different polarizations of the incident wave. In particular, a quasi-TEM wave guide setup, reported in [24] is used to characterize the transmission of surface waves through the structures. As shown in Fig. 3, two main directions are of interest: from left to right (between ports P1 and P2) and in the transverse direction, starting from bottom up (between ports P3 and P4). The main direction (wave vector k parallel to the x axis) corresponds to the coupling direction of the probe-fed patch antennas (array of Fig. 6(a)).

Full wave simulations (scattering parameters) of the proposed designs are performed and some results are presented in Figs. 4 and 5. The electric fields, as indicated in Fig. 3, are always perpendicular to the CSRR's plane in order to exit the electric resonance of the CSRR-based electric materials [16–18]. Fig. 4 (and Fig. 5) shows the transmission across the CSRR structure of Fig. 3(a) (and Fig. 3(d)) to determine its SW stopband frequency. In the main direction of propagation ($k//Ox$), the negative permittivity media have an EM bandgap feature (Figs. 4(a) and 5(a)). As depicted by Fig. 4(a), the CSRR structure of Fig. 3(a) inhibits signal propagation: $S_{21}(\text{dB}) \leq -10 \text{ dB}$ between 5.8 GHz and 6.7 GHz (with a 15% fractional bandwidth). The CSRR structure of Fig. 3(d) has the same

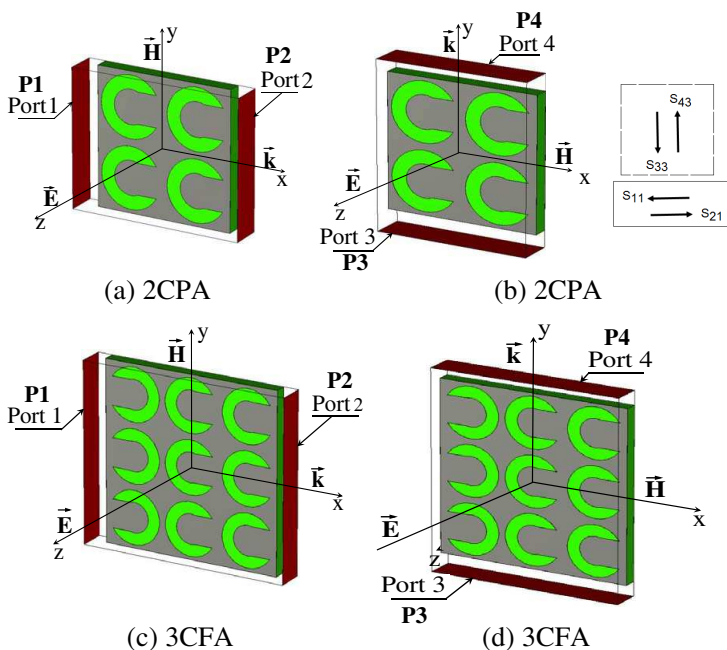


Figure 3. Quasi-TEM wave guide setup. Surface waves (SW) transmission across the MTM array of CSRRs. (a) and (c) propagation from ports P1 to P2 along the main direction ($k//Ox$), and (b) and (d) propagation in the Oy transverse direction from ports P3 to P4 (k is the wave vector).

behavior and presents a wider bandgap in the Ox direction (Fig. 5(a)) between 5.8 GHz and 7.1 GHz (with a $\sim 21\%$ fractional bandwidth).

On the contrary, along the transverse direction ($k//Oy$) the transmission through the two structures is complete with S_{34} (dB) ~ 0 dB between 5.5 GHz and 6.14 GHz (as shown in Figs. 4(b) and 5(b)).

3. MUTUAL COUPLING REDUCTION

Figure 6 presents the experimental setup used to investigate the mutual coupling reduction between two probe-fed adjacent E -coupled patch antennas. The patch antennas dimensions are $a = 0.32\lambda_g$, $b = 0.44\lambda_g$, and $dx = 0.12\lambda_g$. The distance edge-to-edge between the antennas is $d = 0.8\lambda_0$. Here λ_0 and λ_g are the free space and the guided wavelengths for microstrip line at the resonant frequency ($f_0 = 6$ GHz; $\lambda_0 \sim 49$ mm and $\lambda_g = \lambda_0/\epsilon_r^{1/2}$).

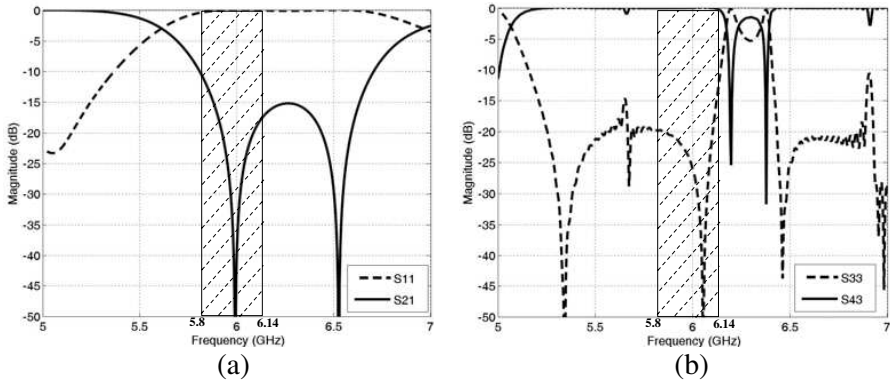


Figure 4. Transmitted and reflected signals of the first CSRR structure (Fig. 3(a)), (a) S_{11} and S_{21} in the main direction of propagation ($k//Ox$): bandgap feature (0.8 GHz) between 5.8 GHz and 6.14 GHz, and (b) S_{33} and S_{43} in the transverse direction ($k//Oy$): full transmission (band-pass) between 5.92 GHz and 6.14 GHz.

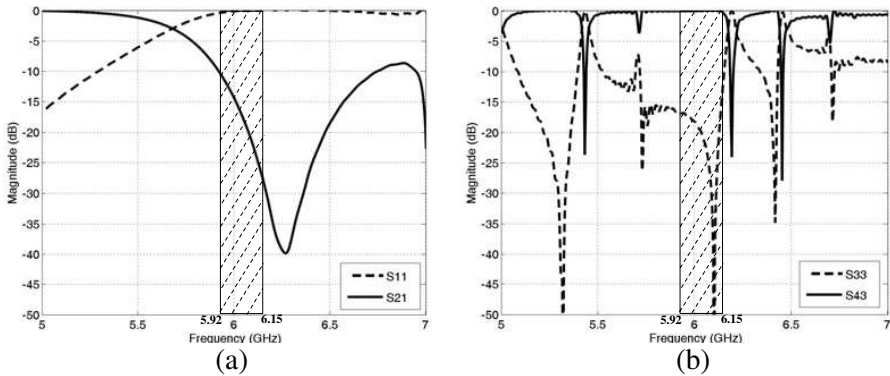


Figure 5. Transmitted and reflected signals of the first CSRR structure (Fig. 3(d)), (a) S_{11} and S_{21} in the main direction of propagation ($k//Ox$): bandgap feature between 5.92 GHz and > 7 GHz (1.18 GHz), and (b) S_{33} and S_{43} in the transverse direction ($k//Oy$): full transmission (band-pass) between 5.92 GHz and 6.15 GHz.

The dielectric substrate is the Rogers RO6010 [28] with $\epsilon_r = 10.2$, loss tangent of 0.001 and 1.9 mm thick. The uniform ground plane has a finite size $L_1 \times L_2 = 2\lambda_0 \times 1.1\lambda_0$ (Fig. 6).

The mutual coupling reduction is investigated by placing the planar MTM structure between the antennas (setup shown in Fig. 6(c)).

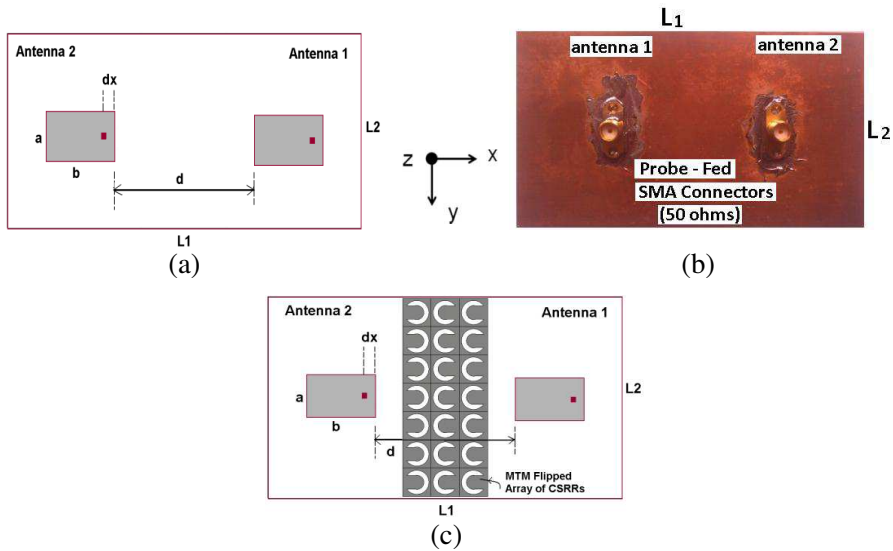


Figure 6. Microstrip antennas array with two *E*-coupled adjacent patch antennas, (a) conventional or simple antennas array, (b) picture of the fabricated array bottom view with the two fed-probe SMA connectors, and (c) the metamaterial CSRR structure is placed at equal distances between the two antennas.

In antenna arrays, the element centre spacing is within one wavelength, the maximum allowed distance without the appearance of unwanted grating lobes array. In our study, characterizing the four isolator filters has been our objective. Therefore, the antennas distance of $0.8\lambda_0$ has become an acceptable solution because it allows the insertion of the double and triple row CSRR structures.

In the same time, the applicability of the propose structure in the case of smaller inter-element distances ($d \leq 0.5\lambda_0$), in phased arrays for example is very important [13, 14]. Hence, simulations with a distance of $0.5\lambda_0$ were performed. However, due to lack space between the two patch antennas, only two rows of CSRR structure were used. The simulations results will be presented in Fig. 8 (S_{11} and S_{21}) and Fig. 15 (Far-field radiation patterns).

3.1. Numerical Analysis

The antennas return-loss (S_{11}) and mutual coupling (S_{21}) are simulated without (conventional case) and with the four CSRR metamaterial structures; then compared results are shown in Figs. 7(a)–(d). Within the frequency bandgap of the EM CSRR

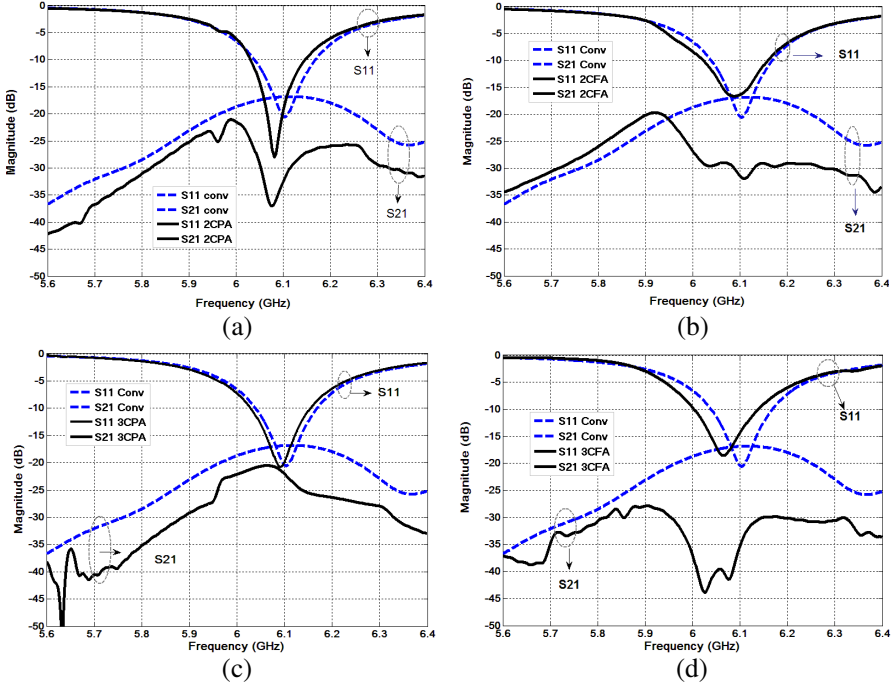


Figure 7. Simulated S_{21} and S_{11} without and with the different metamaterial structures and $d = 0.8 \times \lambda_0$, (a) with the CSRR (7×2) periodic structure (Fig. 2(a)), (b) with the CSRR (7×2) flipped array structure (Fig. 2(b)), (c) with the CSRR (7×3) periodic structure (Fig. 2(c)) and (d) with the CSRR (7×3) flipped array structure (Fig. 2(d)).

structures, strong reduction of the mutual coupling (up to 24 dB) between the adjacent antennas is achieved.

Figure 7(a) gives the simulated results of the first design when the MTM filter is used with the 7×2 periodic CSRR structure (2CPA) of Fig. 2(a). As can be seen in Fig. 7(a), the depth of S_{21} is improved over the entire frequency stopband. The mutual coupling reduction goes from 8 dB to almost 20 dB and $S_{11} = -37$ dB at the resonance (6.1 GHz).

Figure 7(b) shows the simulation results of the antennas array with the second CSRR structure (2CFA) of Fig. 2(b). The S_{21} has a very interesting shape and is quite constant starting from $f = 6$ GHz and over a large frequency band. A mutual coupling reduction of ~ 15 dB is obtained at the minimum of the return-loss. Figs. 7(c)

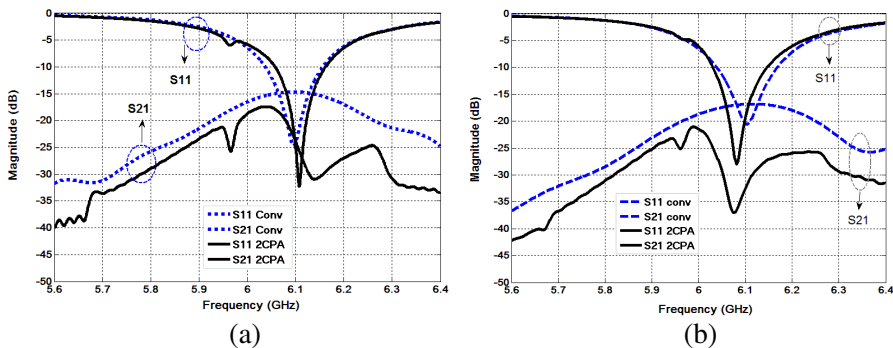


Figure 8. Simulated S_{21} and S_{11} without and with the metamaterial structure of Fig. 2(a), (a) $d = 0.5 \times \lambda_0$ and (b) for comparison $d = 0.8 \times \lambda_0$.

Table 1.

Edge to edge distance d	conventional array (dB) at $f = 6.1$ GHz	2 rows periodic array of CSRRs (dB) at $f = 6.1$ GHz
$0.8\lambda_0$	$S_{11} = -20$ dB $S_{21} = -17$ dB	$S_{11} = -27$ dB $S_{21} = -37$ dB
$0.5\lambda_0$	$S_{11} = -25$ dB $S_{21} = -14$ dB	$S_{11} = -30$ dB $S_{21} = -25$ dB

and 7(d) respectively present the simulation results using the two last structures of Fig. 2(c) (3CPA) and 2(d) (3CFA). Important differences can be observed for S_{21} (level of the minimum and waveforms) between the two designs.

The flipped array of CSRRs ($7 * 3$ unit cells) seems to be efficient in suppressing surface and space waves (Fig. 7(d)). A S_{21} value of -45 dB is obtained inside the metamaterial stopband bandwidth which corresponds to a mutual coupling reduction of 24 dB.

A slightly shift (< 20 MHz) of the resonance frequency is observed between the conventional and the alternative case in the first and fourth cases.

As it was mentioned before, the distance d has been changed from $0.8 \lambda_0$ to $0.5\lambda_0$ for the antenna system. Figs. 8(a) and 8(b) show the simulated S parameters results for the two distances at $f = 6.1$ GHz with and without the MTM slab. Table 1 summarizes in data, the effects of d on the mutual coupling (S_{21}) and reflection coefficient of the antenna (S_{11}).

3.2. Comparison of the CSRRs and Grounded-edge SRR MTM Slabs [11, 13]

The performances of the actual design are compared to those reported by the authors of the reference [11] and more recently [13]. They present a novel MTM slab based on rectangular Grounded Edge-coupled SRR unit cells (GE-SRR) supported by a vertical dielectric substrate. The structure has a large stopband with a 15% fractional bandwidth and allows a mutual coupling reduction of 10 dB at the resonance.

Inspired from those works [11, 13], we design a MTM slab based on circular-type grounded edge-coupled split ring resonator unit cells (CGE-SRR).

For easier comparison with our designs the dielectric substrate [28] has been used. Hence the dimensions of the CGE-SRR particle have been optimized to achieve a resonant frequency around 6.1 GHz. The MTM slab (or vertical isolation wall) with only one row of CGE-SRR was investigated and inserted in the setup of Fig. 6(a) with the same properties: $d = 0.8\lambda_0$ and $f_0 = 6.1$ GHz for the two patch antennas.

Figure 9(a) shows the designed MTM vertical isolation slab with CGE-SRR particles. Fig. 9(b) shows the simulated results. At that distance, the mutual coupling between the patch antenna elements S_{21} is very high in the case of conventional antennas: $S_{21} = -18$ dB at 6.1 GHz. It is reduced by 15 dB while inserting the MTM slab. Moreover the antennas are well matched with a reflection coefficient $S_{11} = -20$ dB at 6.1 GHz. A slight frequency shift of < 20 MHz is

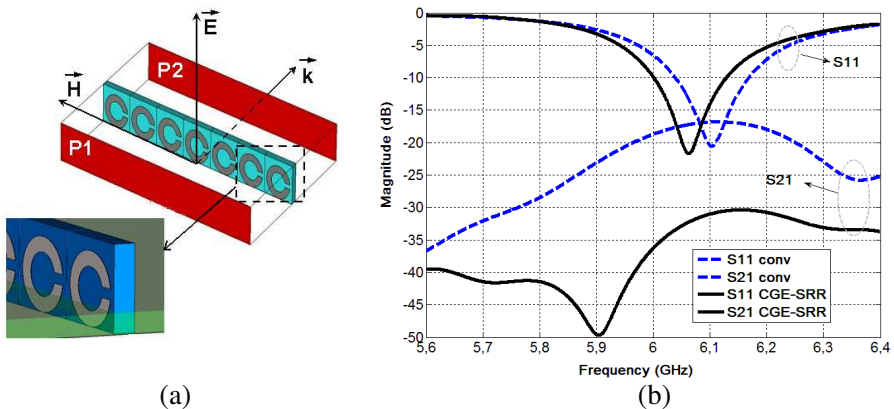


Figure 9. (a) Circular grounded-edge SRR (CGE-SRR) isolation vertical “wall” inspired from [11, 13] and (b) simulated S_{21} and S_{11} with and without the metamaterial array of CGE-SRRs.

Table 2.

MTM Structure	Fractional bandwidth (%)	Mutual coupling reduction (dB)
CGE-SRR	15	15
CSRRs	16	20
Flipped-CSRRs	20	24

observed thanks to the presence of the MTM slab. Table 2 gives a quick comparison between the two MTM isolation slabs.

This comparison demonstrates the compactness, low profile and high efficiency of the actual CSRR designs.

3.3. Experimental Results and Comparison

Figure 10 shows the photographs of the five fabricated prototypes. The first prototype shown in Fig. 10(a) is the conventional array (simple array) without the MTM CSRR and used as a reference. The pictures of Figs. 10 (b)–(e) show the fabricated MTM-based antenna arrays. Here the CSRR isolator filters (structures of Figs. 2(a)–(d) have been placed between the patch antennas. These structures use the same substrate than that described in the simulations. The S parameters are

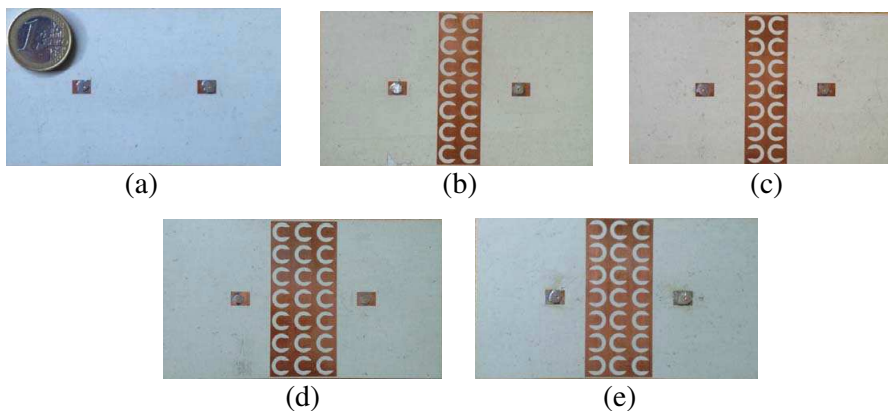


Figure 10. Photographs of the fabricated five prototypes, (a) conventional or simple antennas array, (b) first MTM design with the first isolator filter (Fig. 2(a)), (c) second design with the CSRR filter of Fig. 2(b), (d) third design with the CSRR structure of Fig. 2(c), and the last design with the fourth CSRR structure Fig. 2(d).

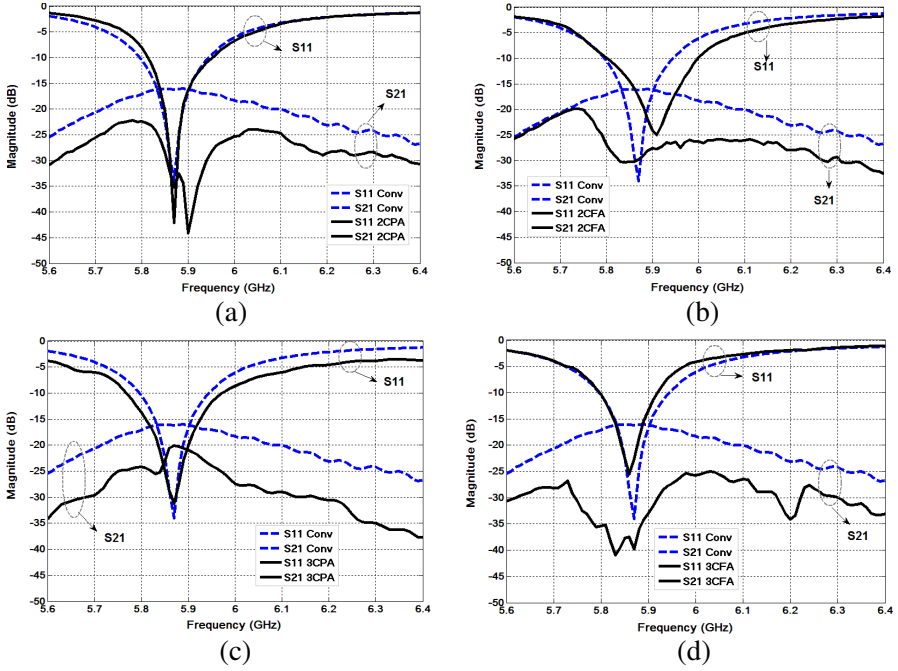


Figure 11. Measured S_{21} and S_{11} without and with the different metamaterial structures and $d = 0.8 \times \lambda_0$, (a) with the CSRR (7×2) periodic structure (Fig. 2(a)), (b) with the CSRR (7×2) flipped array structure (Fig. 2(b)), (c) with the CSRR (7×3) periodic structure (Fig. 2(c)) and (d) with the CSRR (7×3) flipped array structure (Fig. 2(d)).

carefully measured using an Agilent vectorial network analyzer (ENA Series). The experimental results of each MTM design are presented in comparison to the conventional case (reference) in Fig. 11(a) to Fig. 11(d).

All measured results of S_{11} return-loss parameter indicate a resonant frequency at 5.89 GHz (~ 5.9 GHz) whereas the resonant frequency of the simulations is 6.1 GHz (see Figs. 7(a)–(d)). This shift of the frequency is also observed in the reference case, and hence can be attributed to the characteristics of the manufacture dielectric substrate (deviation from data sheet [27] specifications).

Figure 12 illustrates comparisons of the measured and the simulated S_{21} and S_{11} with the different metamaterial structures for $d = 0.8\lambda_0$. Despite the frequency shift, simulated and measured S_{11} and S_{21} (waveforms and depth) are in excellent agreements.

For the conventional antenna (reference case) at 5.9 GHz, the experimental results indicate a high level of the S_{21} with a maximum

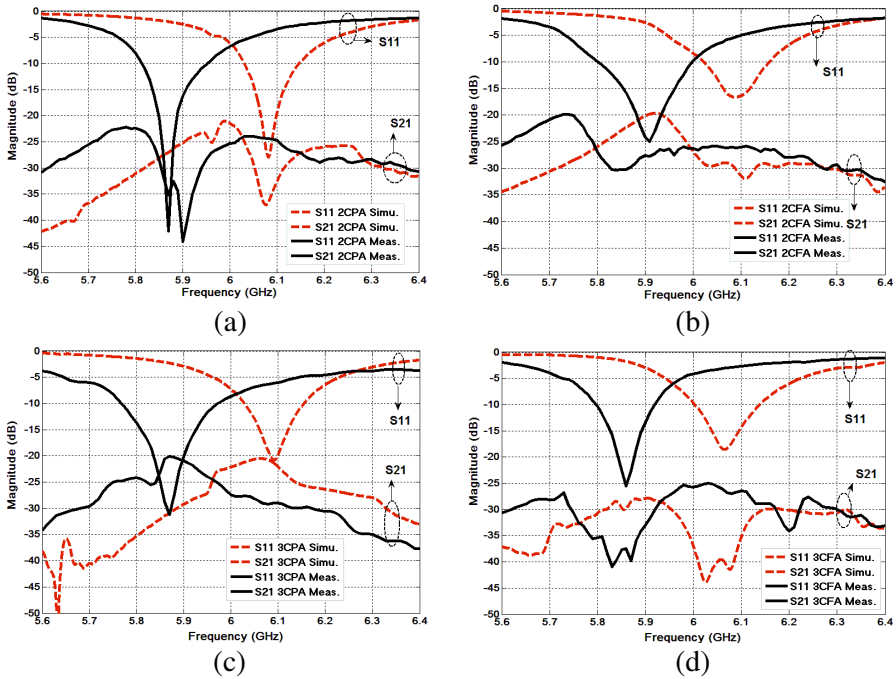


Figure 12. Comparison of the measured and the simulated S_{21} and S_{11} with the different metamaterial structures for $d = 0.8\lambda_0$, (a) with the CSR (7 × 2) periodic structure (Fig. 2(a)), (b) with the CSR (7 × 2) flipped array structure (Fig. 2(b)), (c) with the CSR (7 × 3) periodic structure (Fig. 2(c)) and (d) with the CSR (7 × 3) flipped array structure (Fig. 2(d)). The frequency shift is attributed to a slightly different value of the manufacture dielectric substrates permittivity.

value of -15 dB and good impedance match for the two antennas system $S_{11} = -35$ dB (Fig. 12).

For the entire designs (Figs. 12(a) to 12(d)) one has a significant reduction of the mutual coupling. This underlines the real contribution of the metamaterial CSR inclusions by suppressing the surfaces and space waves (respectively 18 dB, 11 dB, 3.7 dB, and 24 dB).

The measured S_{11} is always below -25 dB corresponding to a good matching for the antennas. However, it is difficult to comment the S_{11} bandwidth which is: slightly narrowed for the first and last structures (Figs. 10(a) and 10(d)) without any frequency shift; enlarged for the others structures (Figs. 10(b) and 10(c)) with a shift of ~ 50 MHz in the case of Fig. 10(b) only as predicted by the simulation results of Fig. 7(b).

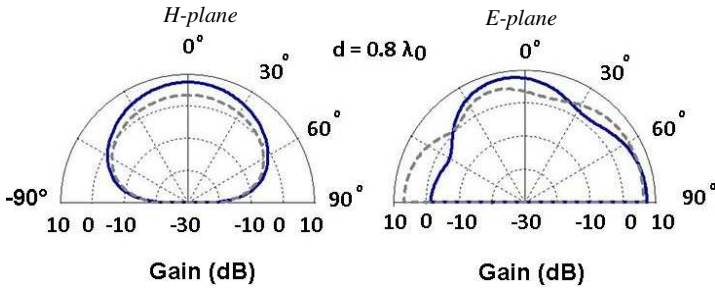


Figure 13. Simulated radiation patterns at 6.1 GHz in E - and H -planes, for $d = 0.8\lambda_0$. Solid line: with the MTM isolator filter (antenna array of Fig. 10(b)) and dashed line: without the MTM (conventional antenna array of Fig. 10(a)).

3.4. Numerical Study of the Radiation Patterns

Far-field radiation patterns of the antenna designs with and without the MTM isolators were numerically determined in the E - and H -planes. For the model, one antenna is active while the other is “passive”; terminated with an impedance of $50\ \Omega$. Fig. 13 presents, an example of the radiation patterns at $f = 6.1$ GHz. Here, the MTM media consists in two rows of periodic array of CSRRs (array antenna Fig. 10(b)). Fig. 13(a) shows the results for $d = 0.8\lambda_0$. The gain of the antenna is increased by 4 dB broadside with an unchanged radiation diagram in the H -plane (Fig. 13(a) left). We notice a deformation of the radiation patterns in the E -plane (Fig. 13(a) right). Thanks to the SW suppression, the radiated field is attenuated by 10 dB in the antenna plane in the side direction to the inserted MTM media ($\theta = -90^\circ$). Thus, Fig. 14(a) shows a high concentration of the surface currents in the loaded passive antenna in the conventional array (Fig. 6(a)) while they are suppressed in Figs. 14(b)–(d) by placing the MTM isolator filters. Fig. 14(c) shows the complete avoidance of SW when using the fourth CSRR structures (Fig. 2(d)) in the antenna array of Fig. 10(e).

Figure 15(a) shows the results for $d = 0.5\lambda_0$. The gain of the antenna is increased by ~ 1.4 dB broadside with an unchanged radiation diagram in the H -plane (Fig. 15(a) left). We notice again a significant deformation of the radiation patterns in the E -plane (Fig. 15(a) right). Here the radiated field is attenuated by 20 dB in the antenna plane at $\theta = -90^\circ$. Finally, a comparison between the radiation pattern in E -plane for the two distances ($d = 0.5\lambda_0$ and $d = 0.8\lambda_0$) is presented in Fig. 15(b). A quite similar far-field radiations behavior in the E -plane can be observed for the two distances.

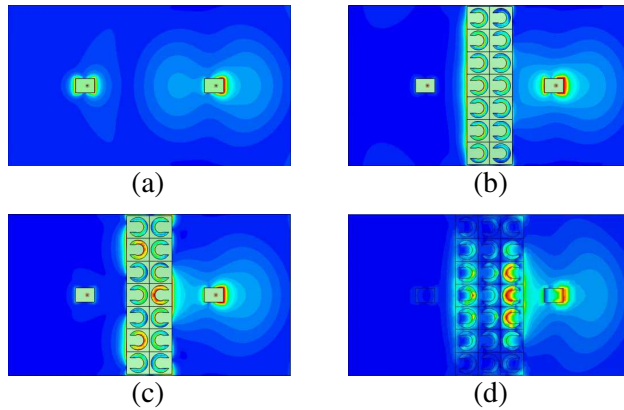


Figure 14. Snapshots of the surface current distribution on the antennas array for $d = 0.8\lambda_0$, (a) conventional (without MTM), and (b), (c) and (d) with MTM array of CSRRs. The presence of the MTM structures allows clearly the SW avoidance on the loaded antenna.

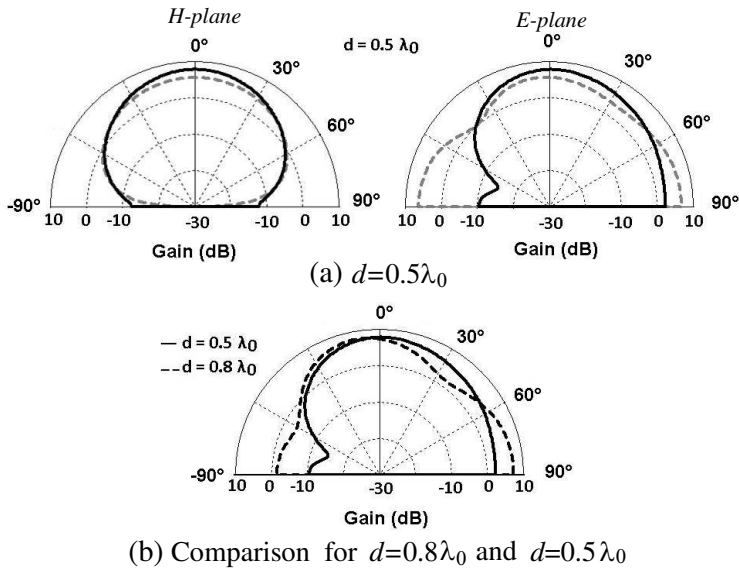


Figure 15. Simulated radiation patterns at 6.1 GHz in E - and H -planes, (a) for $d = 0.5\lambda_0$. Solid line (with MTM isolator filter, antenna array of Fig. 10(b)) and dashed line (without MTM, antenna array of Fig. 10(a)), and (b) E -plane radiation patterns for $d = 0.8\lambda_0$ and $d = 0.5\lambda_0$. Table 3 gives the maximum gain.

Table 3.

	Gain broadside ($\theta=0^\circ$)	<i>E</i> -plane Maximum gain and shape	<i>H</i> -plane Maximum gain and shape
$d=0.8\lambda_0$		Radiation patterns •with deformation	Radiation patterns •without deformation
Without MTM	3.4 dB	6.7dB at $\theta=+45^\circ, -15^\circ, \pm 90^\circ$	3.4 dB at $\theta=0^\circ$
With CSRRs (2CPA)	7.4 dB	7.9 dB at $\theta= -5^\circ, +90^\circ$ and 0 dB at $\theta=-90^\circ$	7.4 dB at $\theta=0^\circ$
$d=0.5\lambda_0$			
Without MTM	6 dB	6 dB (at $\theta=0^\circ, \pm 90^\circ$)	6 dB at $\theta=0^\circ$
With CSRRs (2CPA)	7.4 dB	7.4 dB at $\theta=0^\circ$ and -10 dB at $\theta=-90^\circ$	7.4 dB at $\theta=0^\circ$

4. CONCLUSIONS

In this paper, subwavelength complementary resonators (CSRRs) are used to design microstrip structures with negative permittivity feature. The structures block the EM waves in one direction and guide it in the perpendicular one. Four designs of periodic and flipped arrays of CSRRs are investigated. The objective is to increase the bandwidth of negative permittivity media in order to efficiently suppress both the surface waves (SW) and lateral waves (LW) between two adjacent patch antennas (here the inter-element distance is $d = 0.8\lambda_0$). The flipped array of CSRRs presents a larger bandwidth (relative bandwidth $> 20\%$). By placing the planar isolator filter between the coupled antennas elements, a mutual coupling reduction of 24 dB has been achieved. Moreover, good matching of the antennas is maintained. Without the CSRR's MTM, a high surface current distribution is observed on the loaded antenna. The presence of the MTM structures clearly allows their avoidance. On the other hand, deformation of *E*-plane radiation patterns was observed. The developed isolators' filters are wideband, very efficient in suppressing the surface current and very simple to be implemented in microstrip antenna arrays. The results demonstrate the good potential of the CSRR structures as an efficient EM isolator filter for microstrip phased arrays and MIMO antennas.

ACKNOWLEDGMENT

The authors would like to express their thanks Prof. Omar M. Ramahi from University of Waterloo, Canada for the many discussions and all provided advice.

REFERENCES

1. Sievenpiper, D., L. J. Zhang, R. F. J. Broas, N. G. Alexopolous, and E. Yablonovitch, "High-impedance electromagnetic surfaces with a forbidden frequencyband," *IEEE Trans. on Microw. Theory and Tech.*, Vol. 47, No. 11, 2059–2074, Nov. 1999.
2. Fu, Y. Q., Q. R. Zheng, Q. Gao, and G. H. Zhang, "Mutual coupling reedction between large antenna arrays using electromagnetic bandgap (EBG) structures," *Journal of Electromagnetic Waves and Applications*, Vol. 20, No. 6, 819–825, 2006.
3. Yang, F. and Y. R. Samii, *Electromagnetic Band Gap Structures in Antenna Engineering*, Cambridge University Press, 2009.
4. Karnfelt, C., P. Hallbjorner, H. Zirath, and A. Alping, "High gain active microstrip antenna for 60-GHz WLAN/WPAN applications," *IEEE Trans. on Microw. Theory and Tech.*, Vol. 54, No. 6, 2593–2603, Jun. 2006.
5. Ohnimus, F., I. Ndip, E. Engin, S. Guttowski, and H. Reichl, "Study on shielding effectiveness of mushroom-type electromagnetic bandgap structures in close proximity to patch antennas," *Proc. LAPC*, 737–740, Loughborough, UK, 2009.
6. Nikolic, M., A. Djordjevic, and A. Nehorai, "Microstrip antennas with suppressed radiation in horizontal directions and reduced coupling," *IEEE Trans. on Antennas and Propag.*, Vol. 53, No. 11, 3469–3476, Nov. 2005.
7. Tan, M. N. M., T. A. Rahman, S. K. A. Rahim, M. T. Ali, and M. F. Jamlos, "Antenna array enhancement using mushroom-like electromagnetic band gap (EBG)," *Proc. 4th EuCAP*, 1–5, Barcelona, Spain, Apr. 2010.
8. Coulombe, M., S. F. Koodiani, and C. Caloz, "Compact elongated mushroom (EM)-EBG structure for enhancement of patch antenna array performances," *IEEE Trans. on Antennas and Propag.*, Vol. 58, No. 4, 1076–1086, Apr. 2010.
9. Yang, F. and Y. R. Samii, "Microstrip antennas integrated with electromagnetic band-gap (EBG) structures: A low mutual

- coupling design for array applications,” *IEEE Trans. on Antennas and Propag.*, Vol. 51, No. 10, 2936–2946, Oct. 2003.
10. Li, L., B. Li, H. X. Liu, and C. H. Liang, “Locally resonant cavity cell model for electromagnetic band gap structures,” *IEEE Trans. on Antennas and Propag.*, Vol. 54, No. 1, 90–100, Jan. 2006.
 11. Tang, M.-C., S.-Q. Xiao, S.-S. Gao, G. Jian, and B.-Z. Wang, “Mutual coupling suppressing based on a new type electric resonant SRRs in microstrip array,” *Acta Phys. Sin.*, Vol. 59, No. 3, 1851–1856, 2010.
 12. Tang, M.-C., S.-Q. Xiao, J. Guan, Y.-Y. Bai, S.-S. Gao, and B.-Z. Wang, “Composite metamaterial enabled excellent performance of microstrip antenna array,” *Chin. Phys. B*, Vol. 19, No. 7, 074214, 2010.
 13. Tang, M.-C., S. Q. Xiao, B. Z. Wang, J. Guan, and T. W. Deng, “Improved performance of a microstrip phased array using broadband and ultra-low-loss metamaterial slabs,” *IEEE Antennas and Propagation Magazine*, Vol. 53, No. 6, 31–41, Dec. 2011.
 14. Habashi, A., J. Nourinia, and C. Ghobadi, “Mutual coupling reduction between very closely spaced patch antennas using low-profile folded split-ring resonators (FSRRs),” *IEEE Antennas and Wireless Propagation Letters*, Vol. 10, 862–865, 2011.
 15. Bait-Suwailam, M. M., M. S. Boybay, and O. M. Ramahi, “Electromagnetic coupling reduction in high-profile monopole antennas using single-negative magnetic metamaterials for MIMO applications,” *IEEE Trans. on Antennas and Propag.*, Vol. 58, No. 9, 2894–2902, Sep. 2010.
 16. Falcone, F., T. Lopetegi, J. D. Baena, R. Marques, F. Martin, and M. Sorolla, “Effective negative-epsilon stopband microstrip lines based on complementary split ring resonators,” *IEEE Microwave and Wireless Components Letters*, Vol. 14, 280–282, 2004.
 17. Abdalla, M. A., M. A. Fouad, H. A. Elregeily, and A. A. Mitkees, “Wideband negative permittivity metamaterial for size reduction of stopband filter in antenna applications,” *Progress In Electromagnetics Research C*, Vol. 25, 55–66, 2012.
 18. Khan, S. N., X. G. Liu, L. X. Shao, and Y. Wang, “Complementary split ring resonators of large stop bandwidth,” *Progress In Electromagnetics Research Letters*, Vol. 14, 127–132, 2010.
 19. Bait-Suwailam, M. M., O. F. Siddiqui, and O. M. Ramahi, “Mutual coupling reduction between microstrip patch antennas using slotted-complementary split-ring resonators,” *IEEE Antennas and*

- Wireless Propagation Letters*, Vol. 9, 876, 2010.
20. Bait-Suwailam, M. M., O. F. Siddiqui, and O. M. Ramahi, "Artificial complementary resonators for mutual coupling reduction in microstrip antennas," *Proceedings of the 41st European Microwave Conference, EuMA*, 10–13, Manchester, UK, Oct. 2011.
 21. Lu, H. M., J. X. Zhao, and Z. Y. Yu, "Design and analysis of a novel electromagnetic bandgap structure for suppressing simultaneous switching noise," *Progress In Electromagnetics Research C*, Vol. 30, 81–91, 2012.
 22. Bitzer, A., A. Ortner, H. Merbold, T. Feurer, and M. Walther, "Terahertz near-field microscopy of complementary planar metamaterials: Babinet's principle," *Optics Express*, Vol. 19, No. 3, 2537, Optical Society of America, OSA, Jan. 31, 2011.
 23. Baena, J. D., J. Bonache, F. Martín, R. M. Sillero, F. Falcone, T. Lopetegi, M. A. G. Laso, J. G. García, I. Gil, M. F. Portillo, and M. Sorolla, "Equivalent-circuit models for split-ring resonators and complementary split-ring resonators coupled to planar transmission lines," *IEEE Trans. on Microw. Theory and Tech.*, Vol. 53, No. 4, 1451–1461, Apr. 2005.
 24. Tran, C.-M., H. Hafdallah-Ouslimani, L. Zhou, A. C. Priou, H. Teillet, J.-Y. Daden, and A. Ourir, "High impedance surfaces based antennas for high data rate communications at 40 GHz," *Progress In Electromagnetic Research C*, Vol. 13, 217–229, 2010.
 25. Ouslimani, H. H., X. Han, and T. Zhang, "Analysis and reduction of electromagnetic coupling interferences in microstrip antenna arrays," *Advanced Electromagnetics Symposium, AES*, 16–18, Paris, France, Apr. 2012.
 26. <http://www.ansys.com/Products/Simulation+Technology/Electromagnetics/High-Performance+Electronic+Design/ANSYS+H-FSS>
 27. <http://www.cst.com/content/products/mws/overview.aspx>.
 28. RT/duroid 6006/6010 Dada sheet: <http://www.rogerscorp.com/documents/612/acm/RT-duroid-6006-6010-laminate-data-sheet.aspx>.